WATER RESOURCES RESEARCH, VOL. 22, NO. 13, PAGES 2031–2046, DECEMBER 1986

A Natural Gradient Experiment on Solute Transport in a Sand Aquifer 2. Spatial Moments and the Advection and Dispersion of Nonreactive Tracers

DAVID L. FREYBERG

Department of Civil Engineering, Stanford University, Stanford, California

The three-dimensional movement of a tracer plume containing bromide and chloride is investigated using the data base from a large-scale natural gradient field experiment on groundwater solute transport. The analysis focuses on the zeroth-, first-, and second-order spatial moments of the concentration distribution. These moments define integrated measures of the dissolved mass, mean solute velocity, and dispersion of the plume. Moments are estimated from the point observations using quadrature approximations tailored to the density of the sampling network. The estimators appear to be robust, with acceptable sampling variability. Estimates of the mass in solution for both bromide and chloride demonstrate that the tracers behaved conservatively, as expected. Analysis of the first-order moment estimates indicates that the experimental tracer plumes traveled along identical trajectories. The horizontal trajectory is linear and aligned with the hydraulic gradient. The vertical trajectory is curvilinear, concave upward. The total vertical displacement is small, however, so that the vertical component of the mean solute velocity vector is negligible. The estimated mean solute velocity is identical for both tracers (0.091 m/day) and is spatially and temporally uniform for the first 647 days of travel time. After 647 days of transport, the plume apparently encountered a relatively large-scale heterogeneity in the velocity field, leading to a distinct vertical layering, and slowing the rate of advance of the center of mass of the plume as a whole. The estimated horizontal components of the covariance tensor evolve over time in a manner consistent with the qualitative shape changes observed from plots of the concentration data. The major principal axis, initially aligned roughly perpendicular to the hydraulic gradient, rotates smoothly over time until it is nearly aligned with the mean solute velocity vector, as the plume itself elongates and orients its long axis with the direction of movement. Plots of the components of the covariance tensor as functions of time show evidence of what is commonly called "scale-dependent" dispersion: the rate of growth of the covariance over time is not linear. The theoretical results of G. Dagan (1984) calibrate well to the estimated covariance data for the first 647 days of transport. The calibrated values of the parameters of the hydrualic conductivity distribution closely match independently measured values from the site. The asymptotic longitudinal dispersivity obtained from the calibration is 0.49 m, although asymptotic conditions were apparently not reached. The estimated covariance terms for the last sampling session, 1038 days after injection, are inconsistent with the earlier data and with the Dagan model, particularly for the transverse and off-diagonal components. This behavior is probably attributable to the observed large-scale heterogeneity in the velocity field.

INTRODUCTION

The first paper in this series [*Mackay et al.*, this issue] describes the goals, design, and implementation of a long-term, large-scale, natural gradient field experiment on the transport of inorganic tracers and halogenated organic compounds in groundwater. Achieving the goals for this experiment requires analyses of the experimental data base to obtain information about the spatially averaged movement of the nonreactive, inorganic tracers included in the injected pulse. Such information is especially important in quantifying the relative mass loss and apparent retardation of the halogenated organic solutes, and in attempting to validate mathematical models of dispersive transport.

In this paper we present the results of our initial examination of the tracer data, focusing on (1) the methodology used to obtain quantitative measures of plume size, location, movement, dilution, and spreading, (2) the application of this methodology to the experimental data base, and (3) the interpretation of the results of the analysis. The goals of this work are to extract from the data base quantitative information on the bulk characteristics of the plumes of the nonreactive tracers, including the mass in solution, the location and movement of the center of mass, and the spreading of the plumes about the center of mass (dispersion), and to evaluate the reliability of this information in the context of its intended use.

The methodology developed in this study has also been used to analyze the behavior of the organic compounds included in the experiment; the results of the analysis for mass and the horizontal movement of the center of mass are reported in a separate paper in this series [*Roberts et al.*, this issue]. Another companion paper discusses the spatial variability of aquifer hydraulic conductivity and its relationship to the mean motion described herein [*Sudicky*, this issue].

The next section of this paper describes the experimental data base for the tracers, both its extent and quality. A general description of the procedure for estimating the zeroth-, first-, and second-order spatial moments of concentration distributions using observed point data follows. The remaining sections then present the results of applying this procedure to the tracer data. The paper ends with a summary and discussion which draws some conclusions and which further links this work to its companion papers.

EXPERIMENTAL DATA BASE

As is described in detail in the work by *Mackay et al.* [this issue], the experiment began with a pulse injection of a solution containing two inorganic, nonreactive tracers and five volatile, halogenated organic compounds into a shallow, phreatic aquifer. The aquifer underlies an abandoned sand quarry at Canadian Forces Base Borden in Ontario, Canada.

Paper number 5W4218.
0043-1397/86/005W-4218$05.00

TABLE 1. Nonreactive Tracers in the Experimental Injection Solution

Tracer Ion	Average Concentration, mg/L	Mass Injected, kg	Aqueous Diffusion Coefficient,* m^2/s
Chloride (Cl^-)	892	10.7	2.03×10^{-9}
Bromide (Br^-)	324	3.87	2.08×10^{-9}

*Free ion aqueous diffusion coefficient at 20°C. Taken from *Cussler* [1984].

Table 1 summarizes pertinent information on the nonreactive tracers in the injected solution, including average concentration, total dissolved mass, and the aqueous diffusion coefficient.

Two tracers were used for several reasons. A contaminant plume is known to emanate from an abandoned landfill upgradient from the experimental site [*MacFarlane et al.*, 1983]. This plume, which lies for the most part below the experimental zone, is known to contain elevated concentrations of chloride ion, but negligible concentrations of bromide ion. Inspection of chloride-bromide concentration ratios for the samples collected during the experiment allows identification of any regions in which the experimental and landfill plumes intersect. The use of two nonreactive tracer ions thought to behave identically also provides valuable information on aspects of the sampling variability of the spatial moment estimation technique. In particular, different analysts performed the data reduction for the two ions, allowing observation of any variability introduced by analysts' judgment.

The Borden aquifer material is a relatively homogeneous, medium- to fine-grained sand. Clay size fractions are almost completely absent. The principal forms of spatial heterogeneity observed at the site are thin lenses (0.02–0.10 m) of limited lateral extent (2–5 m) composed of materials of contrasting particle size distribution and hydraulic conductivity [*Sudicky*, this issue]. Both finer-grained and coarser-grained lenses are observed.

TABLE 2. Estimates of Borden Aquifer Properties in the Vicinity of the Experimental Site

	Estimates of Borden Aquifer Properties
Horizontal Hydraulic Gradient Magnitude	
Range	0.0035–0.0056*‡
Annual mean	0.0043‡
Horizontal Hydraulic Gradient Direction	
Range	N40°E to N54°E*‡
Annual mean	N45°E‡
Hydraulic Conductivity¶	
Range	5×10^{-7} to 2×10^{-4} m/s‡
Geometric mean	7.2×10^{-5} m/s‡
Standard deviation of natural log	0.62‡
Isotropic horizontal correlation scale exponential model	2.8 m‡
Vertical correlation scale exponential model	0.12 m‡
Porosity	
Mean	0.33*
Coefficient of variation	0.05*
Apparent Dispersivity (After 11-m Advection)	
Longitudinal	0.08 m†
Horizontal transverse	0.03 m†
Vertical dispersion coefficient	10^{-10} m^2/s†

**Mackay et al.* [1986].
†*Sudicky et al.* [1983].
‡*Sudicky* [this issue].
¶Additional data presented in the work by *Mackay et al.* [this issue].

After injection the plumes of solute moved under the action of the natural gradient at the site. Plume movement was monitored using a dense network of multilevel point samplers [see *Mackay et al.*, this issue, Figure 5]. The spatial and temporal distribution of data collection for the tracers is summarized in Table 4 of *Mackay et al.* [this issue]. In all, over 11,000 samples were collected during 14 synoptic sampling sessions. Elapsed travel time was 1038 days, with the maximum travel distance exceeding 110 m.

The field sampling equipment and protocols are described in detail elsewhere [*Mackay et al.*, this issue]. Because of the careful design of this equipment and the care taken during sample collection and laboratory analysis, the data are believed to be of high quality. The precision of the field and laboratory procedures have been examined quantitatively using replicate field samples routinely drawn from one point on each multilevel sampler during the first eight sampling sessions. The sources of sample variability in this case include (1) small-scale spatial variability of tracer concentration in the immediate vicinity of the sampling point, (2) sample collection and handling, and (3) laboratory analytical procedures (automated ion chromatography). Straightforward statistical analysis of the replicate sample values yields an estimated standard error of measurement of 23 mg/L for chloride and 8 mg/L for bromide. These values are applicable for chloride concentrations greater than 100 mg/L and bromide concentrations greater than 20 mg/L. Below these concentrations, the standard error decreases with decreasing concentration such that the standard error remains roughly a constant percentage of the concentration, about 20% for chloride and 35% for bromide.

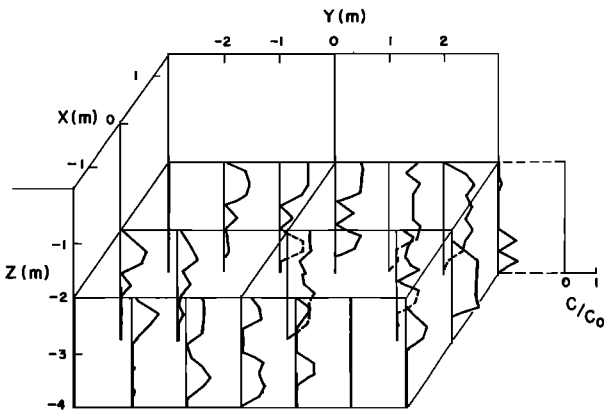

Fig. 1. Relative concentration distribution of chloride at the multilevel sampling wells on August 24, 1982, 1 day after injection. C_o = 892 mg/L (taken from *Mackay et al.* [this issue]).

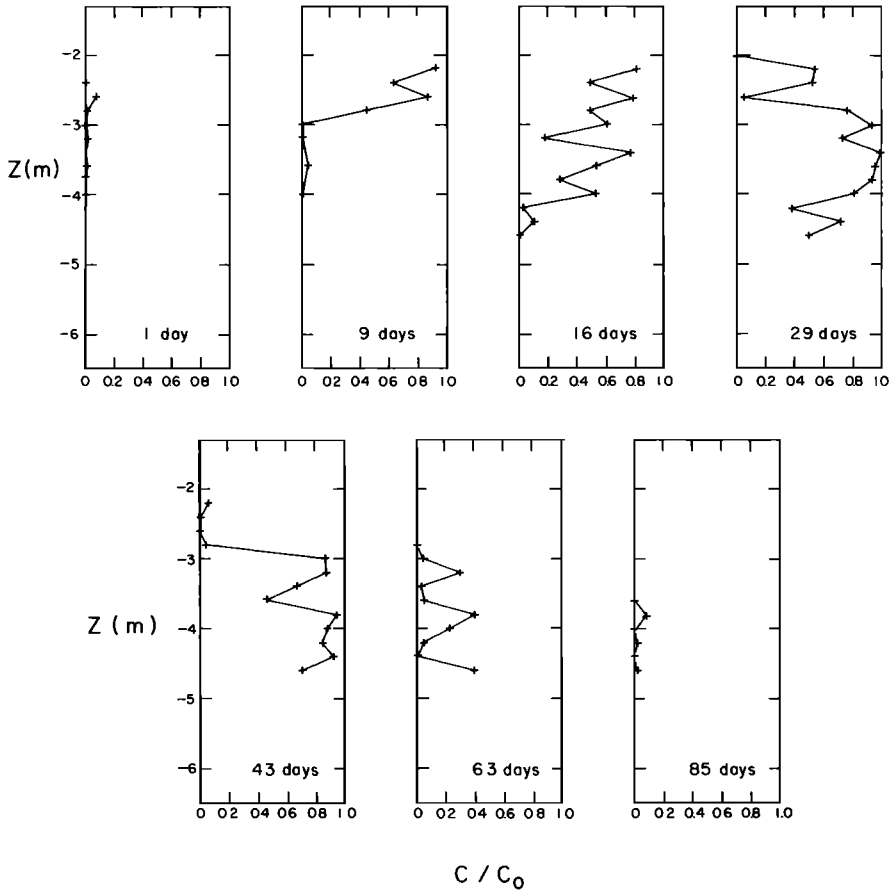

Fig. 2. Time history of the vertical distribution of chloride ion concentration, normalized by the injection concentration, at the sampler located at $x = 2.5$ m and $y = 0.0$ m. $C_0 = 892$ mg/L.

Overview of Plume Behavior

Before examining the spatial moment estimates for the tracers, it is useful to develop a qualitative sense of plume structure and movement. Such an overview provides a sense of the spatial and temporal variability of concentration at scales smaller than the entire plume. It also gives some perspective on the difficulties of spatial moment estimation for this particular data set.

Figure 6 of *Mackay et al.* [this issue], reproduced here as Figure 1, shows the three-dimensional distribution of sampled point concentrations of chloride, normalized by the estimated injection concentration (892 mg/L), 1 day after injection. Inspection reveals both significant small-scale spatial variability, as well as larger-scale structure. At the small scale, relative concentration varies from nearly zero to nearly one over vertical intervals as small as 0.20 m, the resolution of the multilevel samplers. Such variability is consistent with the small-scale vertical variability observed in the hydraulic conductivity field [*Sudicky*, this issue]. Horizontally, vertical distributions of concentration are consistent from sampler to sampler over distances of 3–4 m. This is particularly noticeable in the sampler rows at $x = -1.5$ and at $x = +1.5$ m. Horizontal structure of a similar scale also appears in the hydraulic conductivity field [*Sudicky*, this issue].

At a larger scale, the chloride plume on the day after injection dips somewhat from front to back (in the negative x direction). Although injection was carefully controlled to ensure a reasonably uniform concentration and volumetric flow rate in each of the nine injection wells, the initial distribution of chloride ion is neither symmetric about lines of symmetry in the injection well layout, nor is it smooth.

A second qualitative perspective on plume shape and movement is gained by examination of Figure 2, showing the time history of the vertical distribution of chloride relative concentration at a sampler located in the near field, close to the injection zone ($x = 2.5$ m, $y = 0.0$ m). The concentration profiles of Figure 2 demonstrate the impact of the initial front-to-back dip of the plume and of the small vertical component of velocity at the site. Regions of high concentration, which are initially near the top of the sampling zone, migrate slowly and consistently toward the bottom of the sampling zone over the duration of plume passage. Since the depths at which high concentrations are observed at this sampler after 43 days of transport are somewhat greater than the depths of high concentrations observed at the back of the plume immediately after injection, this migration is a consequence of both the initial shape of the plume and the vertically downward component of mean velocity. Note that the small-scale variability in the vertical concentration structure is present throughout the duration of tracer passage. Since this sampling point is located very close to the injection zone, little or no smoothing occurs.

Figure 8 of *Mackay et al.* [this issue] provides another, more integrated perspective on the qualitative behavior of the tracer plumes over the duration of the experiment. Shown there are equal concentration contour plots of vertically averaged chloride ion concentrations at 1, 85, 462, and 647 days after injection. Initially, the vertically averaged plume is nearly rectangular and unimodal, although significant small-

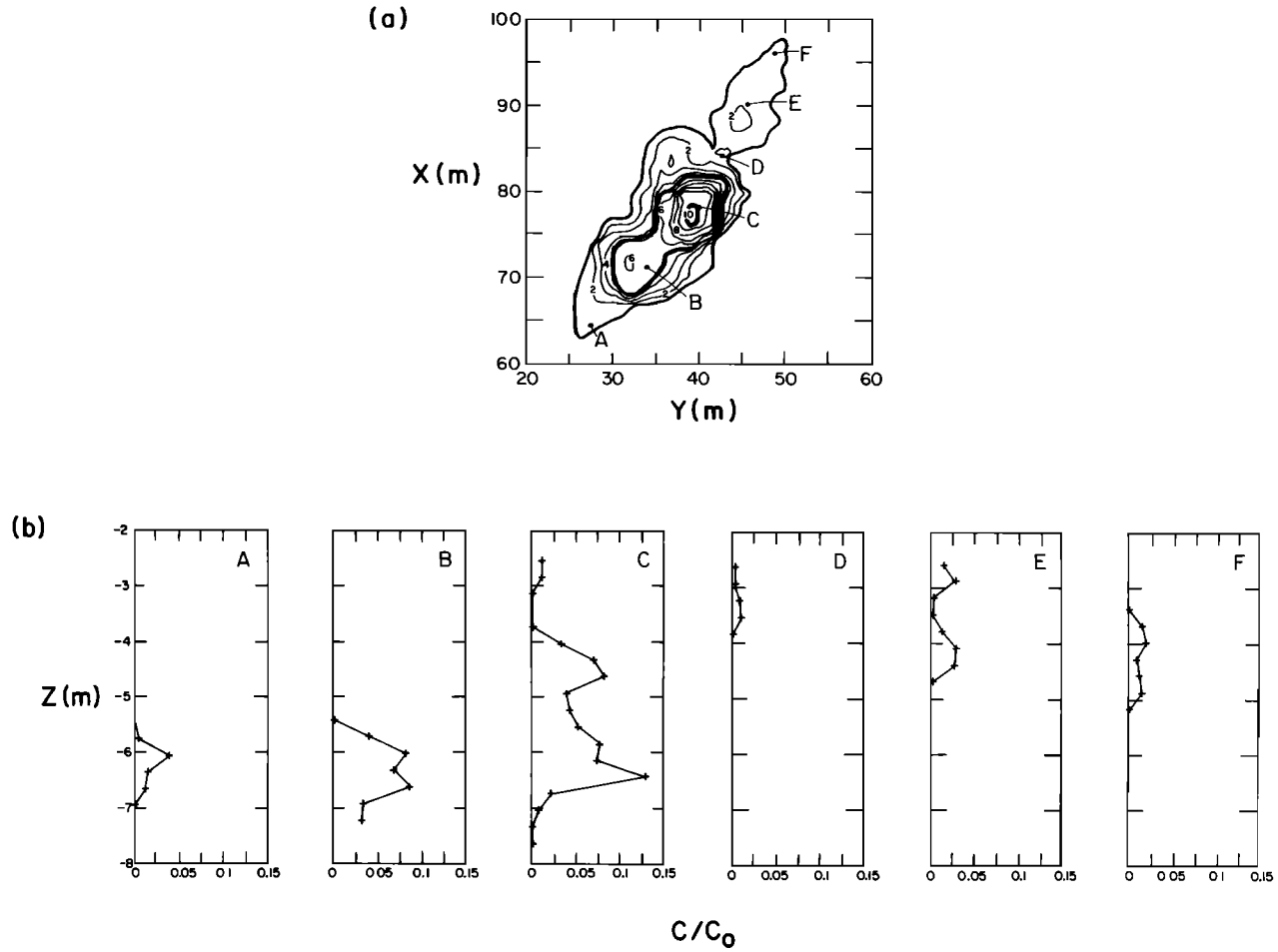

Fig. 3. Distribution of bromide concentration for the last sampling session, 1038 days after injection. (*a*) Vertically averaged concentration contours [mg/L]. (*b*) Vertical distribution of point concentrations, normalized by the injection concentration for six sampling wells along the approximate longitudinal axis of the plume.

scale variability is apparent. Also, the concentration distribution is somewhat skewed in the positive x direction. (Figure 1 shows the point concentrations from which the vertically averaged contour plot for the first sampling session was constructed.) As the plume moves along a nearly linear trajectory at an angle to the field coordinate system, its shape and internal structure are modified. A distinct bimodality in the vertically averaged concentration distribution develops during the first 85 days of the experiment. This bimodal structure persists throughout the next 560 days of the experiment. While the plume appears to develop and maintain a symmetry transverse to the direction of motion, symmetry does not develop in the longitudinal direction. The plume does maintain its integrity as a single plume during this time. However, it does not obtain a Gaussian form.

Accompanying the changes in internal structure, significant spreading occurs in the longitudinal direction and vertically averaged concentrations decrease. However, relatively little horizontal transverse spreading is apparent.

Vertically averaged concentration plots give an incomplete perspective on plume structure and must be interpreted with care. For example, Figure 3 presents a vertically averaged concentration contour plot for bromide for the last sampling session, 1038 days after injection. Also shown on the figure are profiles of the vertical distribution of point concentrations at six samplers along the approximate centerline of the plume. The bimodal structure observed in Figure 8 of *Mackay et al.* [this issue] for earlier sampling sessions is further developed at this time, to the point where future splitting of the plume into two subplumes might be anticipated. Examination of the vertical concentration distributions reveals that the bimodal structure is apparently caused by vertical separation of the plume into two layers. The larger, upstream segment of the plume is found in the bottom points of the sampling wells. The smaller, downstream segment is found in the upper points at higher elevations. The two layers appear to overlap at sampler C. This structure suggests that in this region of the aquifer the mean horizontal velocity decreases with depth, tending to shear the plume into two layers. This in turn gives rise to the observed bimodal form for the vertically averaged concentration distribution.

It is interesting to recall that the vertical structure of the plume immediately after injection exhibited an upstream dip (see Figures 1 and 2 and previous discussion). Figure 9 of *Mackay et al.* [this issue] presents contour plots of the concentration distribution over a vertical cross section through the longitudinal centerline of the plume for 1 and 462 days after injection. The upstream dip is seen to be a consistent pattern throughout the experiment, becoming more pronounced over time and distance. Furthermore, this structure persists even though the plume as a whole is displaced downward over several meters. Very little vertical spreading occurs, however, with the thickness of the plume increasing only slightly over 1038 days of transport.

To summarize, the initial concentration distribution, occupying about 36 m^3 of aquifer, was characterized by significant vertical variability, with horizontal continuity observed over distances of 3–4 m. The plume dipped somewhat from front to back. As the plume moved downgradient along a nearly linear horizontal trajectory, it spread significantly in the longitudinal direction, somewhat in the horizontal transverse direction, and very little vertically. The vertically averaged concentration distribution became bimodal after about 85 days of travel time and remained so for the remainder of the experiment. The distribution did not become Gaussian. The upstream dip in the vertical structure of the plume persisted throughout the experiment, even though the plume as a whole was displaced downward over a distance of several meters. By the last sampling session, the plume appeared to be separating vertically into two layers, with the upper layer traveling at a slightly greater velocity than the lower layer.

The following sections provide a quantitative assessment of a number of aspects of the preceding qualitative description of plume movement, using spatial moment estimates. The discussion begins with an explanation of the moment estimation techniques.

SPATIAL MOMENT ESTIMATION

As is demonstrated in Figures 1, 2 and 3, the point observations of tracer concentration show considerable variability in space and time, which can be attributed to small-scale variability in the hydraulic properties of the Borden aquifer and measurement noise introduced by field sampling and laboratory analysis. For many applications, such as identifying loss of mass in solution over time or assessing dispersive transport model formulations, larger-scale, integrated measures of solute motion are useful, and often most appropriate. Spatial moments of the point concentration distribution provide such measures [*Aris*, 1956].

Spatial Moments

The *ijk*th moment of the concentration distribution in space, $M_{ijk}(t)$, is defined here, after *Aris* [1956] as

$$M_{ijk}(t) = \int_{-\infty}^{\infty}\int_{-\infty}^{\infty}\int_{-\infty}^{\infty} nC(x, y, z, t)x^i y^j z^k \, dx \, dy \, dz \qquad (1)$$

where $C(x, y, z, t)$ is the concentration field (above background); n is the porosity; and x, y, z are the spatial coordinates. The volume integral of (1) is defined over all space. However, the integrand will be nonzero only over regions where the concentration $C(x, y, z, t)$ is nonzero. Therefore the spatial moment $M_{ijk}(t)$ is an integrated measure of the concentration field over the extent of the solute plume. The term "plume scale" will be used here to indicate this property of the spatial moments.

In this paper, we focus on the zeroth, first, and second moments ($i + j + k = 0$, 1, or 2, respectively). These moments provide measures of the mass, location, and spread of the tracer plumes. They also arise naturally in the parameterization of many mathematical transport models, as described below. These lower-order moments do not, of course, completely describe plume structure. Higher-order moments can be used to examine, for example, the skew or kurtosis of concentration distributions. Under some circumstances such information may be essential to the complete characterization and interpretation of solute movement. Unfortunately, it is very difficult to develop reliable estimators for the higher-order moments. Therefore examination of moments of order greater than two is not pursued in the present study.

Physically, the zeroth moment M_{000} is equal to the mass of tracer in solution. For a pulse input of an ideal, nonreactive tracer the mass in solution must remain constant over time.

The first moment about the origin, normalized by mass in solution, defines the coordinate location of the center of mass (x_c, y_c, z_c):

$$x_c = M_{100}/M_{000} \quad y_c = M_{010}/M_{000} \quad z_c = M_{001}/M_{000} \qquad (2)$$

We then define the mean velocity vector $\mathbf{U}$ as the time rate of change of the displacement of the center of mass:

$$\mathbf{U} = \left[\frac{dx_c}{dt}, \frac{dy_c}{dt}, \frac{dz_c}{dt}\right]^T \qquad (3)$$

Note that as defined by (3), $\mathbf{U}$ is a plume-scale average solute velocity. Under the assumptions of a steady, homogeneous pore water velocity field, a pulse input of solute, and transport governed by the classic advection-dispersion model, $\mathbf{U}$ is equal to the pore water velocity. It is common in practice to assume that for transport in a heterogeneous pore water velocity field the average solute velocity is also equal to the average pore water velocity. Several investigators [*Güven et al.*, 1984; *Sudicky*, 1983] have demonstrated this equality for a fully penetrating, instantaneous line source in a perfectly stratified aquifer. However, *Sudicky* [1983] has shown that equality exists for point sources or partially penetrating line sources only for asymptotically large values of time. The two velocities become equal only after the solute plume has spread enough vertically so that it fully reponds to the complete velocity distribution.

Analogous results have been obtained for stochastic models of field-scale transport [*Gelhar et al.*, 1979; *Matheron and de-Marsily*, 1980; *Simmons*, 1982; *Dagan*, 1984]. However, in this case averages represent ensemble means and the issue of ergodicity must usually be considered. As is discussed by *Sposito et al.* [1986], the relationship between $\mathbf{U}$ and the ensemble mean velocity appearing in a number of stochastic models of field-scale transport [e.g., *Gelhar and Axness*, 1983; *Dagan*, 1984] is not well understood. However, several investigators have assumed that $\mathbf{U}$ and the ensemble mean velocity are effectively equal when comparing their models to field data [*Gelhar and Axness*, 1983; *Dagan*, 1984].

The second moment about the center of mass defines a spatial covariance tensor:

$$\boldsymbol{\sigma} = \begin{bmatrix} \sigma_{xx} & \sigma_{xy} & \sigma_{xz} \\ \sigma_{yx} & \sigma_{yy} & \sigma_{yz} \\ \sigma_{zx} & \sigma_{zy} & \sigma_{zz} \end{bmatrix} \qquad (4)$$

$$\sigma_{xx} = \frac{M_{200}}{M_{000}} - x_c^2 \quad \sigma_{yy} = \frac{M_{020}}{M_{000}} - y_c^2 \quad \sigma_{zz} = \frac{M_{002}}{M_{000}} - z_c^2$$

$$\sigma_{xy} = \sigma_{yx} = \frac{M_{110}}{M_{000}} - x_c y_c \qquad \sigma_{xz} = \sigma_{zx} = \frac{M_{101}}{M_{000}} - x_c z_c$$

$$\sigma_{yz} = \sigma_{zy} = \frac{M_{011}}{M_{000}} - y_c z_c$$

In direct analogy with their interpretation in probability theory [compare *Morrison*, 1976], the components of the covariance tensor are physically related to the spread of a concentration distribution about its center of mass. Under the assumptions of a steady, homogeneous pore water velocity field, a pulse input of solute (of arbitrary shape), and transport

governed by the classic advection-dispersion model, integration of the transport equation leads to the following relationship between the dispersion coefficient tensor and the time rate of change of the covariance tensor [*Aris*, 1956]:

$$\mathbf{D} = \frac{1}{2}\frac{d}{dt}(\boldsymbol{\sigma}) \tag{5}$$

Under conditions of a spatially variable pore water velocity field, the term "dispersion" appears to be most commonly used in the physical sense to refer to all deviations in observed or predicted concentration from that which would be predicted assuming only advection by an average pore water velocity field [compare *Bear*, 1972; *Anderson*, 1979; *Simmons*, 1982]. In the general case, these deviations cannot necessarily be fully characterized by the rate of change of the spatial covariance structure of a plume. Higher-order moments may be required. However, a number of investigators have defined an effective or apparent dispersion coefficient using the relationship given in (5) (see, for example, *Aris* [1956], *Sudicky* [1983], and *Güven et al.* [1984]). Both *Sudicky* [1983] and *Güven et al.* [1984] have shown that a dispersion coefficient so defined is not a constant, fixed material property for the case of a perfectly stratified aquifer.

Investigators using stochastic models of field-scale transport have used expressions analogous to (5) to define apparent dispersion coefficients [*Gelhar et al.*, 1979; *Matheron and deMarsily*, 1980; *Dagan*, 1984]. In these studies $\boldsymbol{\sigma}$ is defined as the ensemble covariance tensor, and therefore the apparent dispersion coefficient is also an ensemble property. Results similar to those for perfectly stratified aquifers with deterministic velocity heterogeneities are found: the apparent dispersion coefficient is not a constant, fixed material property. *Sposito et al.* [1986] have described the difficulties in comparing ensemble properties to analogous properties defined over a particular aquifer.

It is common to assume that the dispersion coefficient tensor is related to the pore water velocity through a relationship of the form [*Bear*, 1972]

$$\mathbf{D} = D_d\mathbf{I} + \mathbf{A}|\mathbf{V}| \tag{6}$$

where D_d is the molecular diffusion coefficient of the solute in the porous medium; $\mathbf{I}$ is an identity matrix; $|\mathbf{V}|$ is the magnitude of the velocity vector; and $\mathbf{A}$ is the dispersivity tensor. The coordinate system is assumed to be aligned with the mean velocity vector. For field-scale transport D_d is often assumed to be negligibly small, yielding a simple definition for an apparent dispersivity in terms of the covariance tensor [*Güven et al.*, 1984]:

$$\mathbf{A} = \frac{1}{2|\mathbf{V}|}\frac{d}{dt}(\boldsymbol{\sigma}) \tag{7}$$

Considerable attention has been devoted to the asymptotic, large-time behavior of apparent dispersivity, particularly since a number of models indicate that field-scale transport is asymptotically Fickian (constant $\mathbf{A}$).

Moment Estimation

The magnitudes of the spatial moments and their derived parameters must be estimated from a discrete set of sampled point concentrations. "Point" here refers to the average concentration over a sampling volume of approximately 184 mL of aquifer (70 mL of pore space). Many different estimators can be formulated for the spatial moments and their associated transport parameters. The formulation of the estimators used here was guided by consideration of several issues. First, since one of the goals of the experiment was to develop a data base for testing transport model formulations, we wished to construct estimators that were relatively independent of model assumptions. For example, estimates of transport parameters are often obtained by fitting analytical or numerical solutions of the classic advective-dispersive transport model to experimental data. However, testing an hypothesis of the applicability of the classic model would be very difficult using such estimators, since they are dependent on the classic model assumptions.

A second issue is the statistical properties of the estimators. In particular, we sought relatively unbiased estimators with sampling variances as small as feasible. However, careful quantification of the sampling properties of the estimators is a complex task and was considered beyond the scope of this inital data analysis. Therefore no attempt was made to identify optimal estimators at this stage of the analysis. However, the data base should provide an excellent resource for further exploration of moment estimators. Finally, we wished to identify estimators that could be applied easily, quickly, and as automatically as possible to a large data base by several different analysts.

Methodology

Estimating spatial moments and their derived parameters requires approximating the volume integral in (1) using discrete data. Because of the relatively small amount of vertical displacement and the very slight amount of vertical spreading observed during the experiment (see Figure 9 of *Mackay et al.* [this issue]), an estimation methodology was developed first for the zeroth-, first-, and second-order moments for which the exponent k in (1) is zero. In this case, (1) can be written as

$$M_{ijk}(t) = \int_{-\infty}^{\infty}\int_{-\infty}^{\infty} nC_z(x, y, t)x^i y^j\,dx\,dy \tag{8}$$

with C_z defined as

$$C_z = \int_{-\infty}^{\infty} C(x, y, z, t)\,dz \tag{9}$$

Because the spatial resolution of the data is much greater in the vertical than in the horizontal, a different approximation is used for the integration over the vertical coordinate z than is used for the integration over the horizontal coordinates x and y. The integration over z in (9) is approximated using trapezoidal quadrature. The limits of the integration are set to uniform elevations above and below the plume. For the tracers these elevations are given by $z = -1.5$ m and $z = -7.5$ m, for a total vertical extent of 6.0 m. This is, of course, much greater than the vertical extent of the tracer plumes at any particular point in time or space, but it is convenient because of the vertical movement of the plumes over the duration of the experiment. For locations where the uppermost or lowermost sampling point measured a concentration greater than background, the concentration is assumed to reach background within a distance less than or equal to twice the vertical sampling interval.

A by-product of this step in the estimation process is the vertically averaged concentration $\bar{C}_z(x, y, t)$

$$\bar{C}_z = \frac{1}{b_2 - b_1}\int_{b_1}^{b_2} C(x, y, z, t)\,dz \tag{10}$$

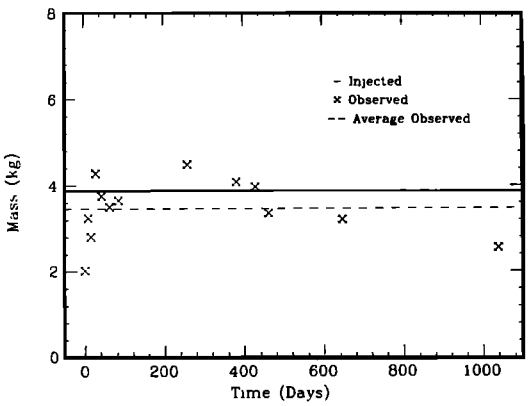

Fig. 4. Estimated mass in solution of bromide ion as a function of time since injection.

where b_1 and b_2 define the top and bottom of the averaging interval. $\bar{C}_z(x, y, t)$ is useful for two-dimensional graphical representations of the plumes, such as those shown in Figure 3 of this paper and in Figure 8 of *Mackay et al.* [this issue].

The density of the sampler network in the horizontal plane is relatively low and spatially nonuniform. As a result, numerical approximations to the integration over the horizontal coordinates in (8) based on polynomial interpolation of the calculated C_z values (such as with trapezoidal rule or Simpson's rule analogs) are quite unstable. For example, estimates of M_{000} (the mass in solution) based on such approximations are very sensitive to individual values of C_z and exhibit large variance over the 14 sampling sessions. Improved performance is obtained by using a more heuristic interpolation, as is described in the following paragraph.

The values of C_z approximated by the quadrature over z at each sampler location are used to estimate $C_z(x, y)$ on a regular, square grid over the horizontal extent of the plume. The basis for this estimation is the SURFACE II Graphics System package of *Sampson* [1978]. The value at a grid node is determined by projecting along the estimated slope of the $C_z(x, y)$ distribution at the four nearest neighboring data points to the grid node location. Projected values are then weighted inversely by the distance, or in some cases the squared distance, between the node and the data point, and averaged. Slopes of the $C_z(x, y)$ distribution are estimated using local planar fits to the data point and its four nearest neighbors. Grid spacing ranges from 0.6 m for the early synoptic sampling sessions, to 1.2 m for sampling sessions in 1983–1985. The grid spacing is therefore maintained at about one fourth to one half the sampler spacing. The estimation of a spatial moment is then completed by approximating the areal integration in (8) with a nine-node, locally fourth-order, areal quadrature of the regular grid of estimated values of C_z [*Abramowitz and Stegun*, 1970, equation 25.4.62].

Any spatial moment estimation methodology incorporates, either explicitly or implicitly, a smoothing or filtering of the concentration distribution. Here, that smoothing is introduced by the choice of trapezoidal quadrature over the vertical and by the grid interpolation and areal quadrature over the horizontal. Unfortunately, existing theory is inadequate to define the spatial structure of concentration variability (for example, via a covariance function or semivariogram) for scales smaller than the monitoring network spacing and under the conditions of this experiment. Also, the probable nonstationarity of the concentration variability over space and time [compare *Gelhar and Axness*, 1983; *Dagan*, 1984] and the relatively sparse sampling network make empirical inference of the functional form of spatial variability at larger scales very difficult. Therefore a moment estimation technique using an explicit model of concentration spatial variability was not developed, and the implicit smoothing introduced by the estimation methodology used in this study has been evaluated only qualitatively.

The estimated values of the coordinates of the center of mass and of the components of the covariance tensor are quite insensitive to the type of quadrature used in either the horizontal or vertical. They are also insensitive to the grid spacing and the spatial weighting used in the interpolation of $C_z(x, y)$. This insensitivity arises because these parameters are ratios of the moments, M_{ijk}. Estimates of the M_{ijk} are themselves somewhat sensitive to the type of smoothing used in the estimation. This sensitivity increases with the order of the moment, as expected. However, because they use the same quadrature and the same smoothing, the moment estimates for a given plume tend to be highly correlated. For example, increased smoothing tends to increase the estimated values of both M_{000} and M_{100} such that their ratio x_c changes very little. As a result, estimates of the location of the center of mass and of the covariance tensor show little sensitivity to smoothing. Estimates of the mass in solution, M_{000}, do show some sensitivity to smoothing assumptions. However, extensive experimentation with the degree of smoothing employed in the estimation of M_{000} never resulted in changes of more than 10%.

Throughout the application of the estimation methodology, porosity was treated as spatially uniform with a mean value of 0.33. As a result, porosity cancels out of all parameter estimates except the mass in solution. Local porosity measurements in the vicinity of each sampling point would be required in order to include porosity in the integrand of the approximations to (1). Unfortunately, it was not possible to obtain such information in the field. Furthermore, because of the difficulty in obtaining undisturbed core samples from depth in the aquifer, relatively few data are available to evaluate statistically the spatial variability of porosity. Data from 0.15-m increments taken from two cores with a total length of 5.19 m yield an estimated coefficient of variation for porosity of 0.05. Based on this small value, porosity was approximated as uniform. Such an approximation can of course increase the variability and bias of the parameter estimates.

Issues, both statistical and practical, in the application and performance of the spatial moment estimators are discussed in the following sections on individual moment estimates. In general, the estimators performed satisfactorily, although it is quite difficult to evaluate quantitatively this performance.

MASS IN SOLUTION

As shown above, the zeroth spatial moment of the concentration distribution measures the mass of a constituent in solution. All evidence to data indicates that the two tracers, chloride and bromide, are nonreactive with the Borden aquifer material. Therefore except for the mass removed during sampling, we expect the mass in solution in the aquifer to be constant over time. Although we have collected nearly 10,000 samples from within and around the chloride and bromide plumes, our best estimate is that we have removed less than 1% of the total mass of the chloride or bromide ions. Thus we do not expect our sampling process itself to have resulted in a measureable loss of mass over time. The measureable mass in solution will of course decrease over time as a larger and larger fraction of the mass is diluted to concentrations which cannot be distinguished from background values.

Figure 4 depicts the estimated mass in solution of bromide

TABLE 3. Estimates of Mass in Solution, Location of Center of Mass, and Spatial Covariance for the Bromide and Chloride Plumes

Date	Elapsed Time, days	Mass in Solution, kg	Center of Mass*			Spatial Covariance†		
			x_c, m	y_c, m	z_c, m	$\sigma_{x'x'}$, m^2	$\sigma_{y'y'}$, m^2	$\sigma_{x'y'}$, m^2
			Bromide					
Aug. 24, 1982	1	2.02	0.3	−0.2	2.78	1.8	2.0	0.4
Sept. 1, 1982	9	3.25	0.6	0.4	2.95	2.3	2.8	1.0
Sept. 8, 1982	16	2.81	1.7	0.9	3.02	1.9	2.8	0.9
Sept. 21, 1982	29	4.29	2.7	1.0	3.34	2.4	2.5	0.9
Oct. 5, 1982	43	3.76	4.1	1.5	3.36	3.6	2.5	0.8
Oct. 25, 1982	63	3.50	5.8	2.2	3.54	4.9	2.7	1.1
Nov. 16, 1982	85	3.66	7.7	2.9	3.80	5.2	2.6	0.3
May 9, 1983	259	4.49	22.9	11.3	4.80	16.7	4.6	2.8
Sept. 8, 1983	381	4.08	31.9	15.1	5.17	20.8	5.0	3.2
Oct. 26, 1983	429	3.97	36.2	17.2	5.30	22.0	7.3	1.9
Nov. 28, 1983	462	3.36	38.4	17.2	5.32	30.1	6.6	2.8
May 31, 1984	647	3.21	53.8	24.6	5.49	50.1	6.9	2.4
June 26, 1985	1038	2.55	77.8	38.1	5.31	83.3	18.8	13.6
			Chloride					
Aug. 24, 1982	1	6.7	0.2	0.1	2.78	2.1	2.4	0.5
Sept. 1, 1982	9	9.2	0.7	0.4	3.02	1.7	2.4	0.7
Sept. 8, 1982	16	9.2	1.6	0.7	3.06	2.3	2.8	0.8
Sept. 21, 1982	29	11.5	2.9	0.9	3.27	2.5	2.6	0.9
Oct. 5, 1982	43	11.3	4.1	1.6	3.34	4.4	2.7	1.2
Oct. 25, 1982	63	9.0	5.7	2.0	3.50	4.4	2.4	1.1
Nov. 16, 1982	85	11.2	7.7	3.2	3.75	5.7	3.3	0.8
May 9, 1983	259	11.5	22.7	11.6	4.52	17.8	4.4	3.7
Sept. 8, 1983	381	9.6	32.3	15.3	5.18	20.6	4.4	3.9
Oct. 26, 1983	429	9.2	35.9	17.2	5.25	24.3	6.0	3.2
Nov. 28, 1983	462	8.2	38.2	17.4	5.33	27.8	5.5	2.1
May 31, 1984	647	9.1	53.1	23.9	5.55	51.5	5.5	3.0

*Given in the field coordinate system.

†Given in rotated coordinates: x' is parallel to linear horizontal trajectory, y' is perpendicular to linear horizontal trajectory.

ion as a function of time since injection. Shown along with the individual data points are the estimated mass injected and the sample mean of the 13 mass estimates. The data for Figure 4 are given in Table 3. As is noted above, the observable mass in solution is expected to be effectively constant over the duration of the experiment. The mass estimates shown on Figure 4 generally confirm this expectation. The estimates for the last six sampling sessions do suggest a downward trend over time. However, the magntiude of this trend is much larger than would be expected from the effects of the mass removed by sampling or from dilution below the analytical detection limit. Therefore this behavior is presumed to be coincidental.

The magnitude of the sampling variability is expected to be directly related to the density of the sampling network within the plume and to the magnitude and spatial structure of concentration variations. For example, the mass estimate for the initial sampling session is quite low, approximately 52% of the injected mass. This may be attributed to the relatively low number of sampling points (158) within the plume, to the fact that the plume extended above the uppermost points on a number of the samplers, and, most importantly, to the lack of sampler density near the center of the plume (see Figure 1). Subsequent sampling sessions revealed that regions of high concentrations existed in the vicinity of the plume center during the first weeks of the experiment. However, the horizontal extent of these regions was smaller than the separation between samplers. Therefore they went undetected during the first sampling session and the mass estimate is low.

The eighth sampling session, 259 days after injection, provides a contrasting example. The mass estimate for this session is rather high, 116% of the injected mass. At this point, the plume was located in the least dense portion of the sampling network (center of mass at $x = 22.9$ m, $y = 11.3$ m, see Figure 5 of *Mackay et al.* [this issue]), and only 82 sampling points were located within the plume. Relatively high concentrations were sampled at those points, however. In the discrete, numerical approximation of the integral in (1), the influence of these high concentrations is distributed over a relatively large fraction of the plume volume, and a high mass estimate results.

One of the original goals in the design of the sampling network was to adjust the sampling density over space to maintain uniform estimation variances (for the central moments) over space and time. Available transport theory at the time provided few quantitative design guidelines. Because of the thin vertical layering of the aquifer sediments (vertical correlation scale of the natural log of hydraulic conductivity $\simeq 0.12$ m), and the horizontal continuity of the lenslike structure of the layers (horizontal correlation scale $\simeq 2.8$ m), the vertical sampling density was set much smaller than the horizontal. Both the vertical and horizontal densities were allowed to decrease downgradient in response to increasing plume size. The horizontal density was allowed to decrease more than the vertical because little vertical spreading was expected. However, this pattern was modified in response to ongoing data analysis and field logistics, and the horizontal density was increased between $x = 38$ m and $x = 64$ m.

Because of the variable horizontal sampling density and because the network did not completely encompass the entire plume for a few of the synoptic sampling sessions, the esti-

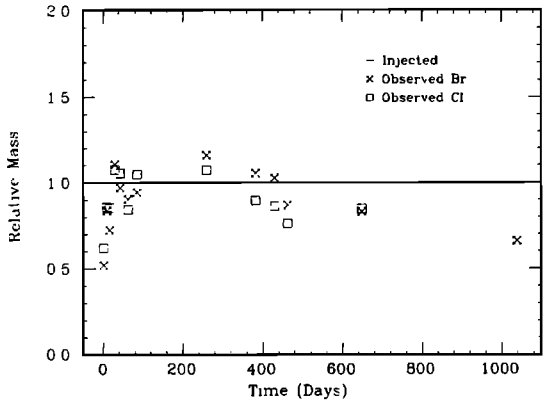

Fig. 5. Estimated masses in solution of chloride and bromide, normalized by injected mass (10.7 kg for chloride, 3.87 kg for bromide).

mation variance for the mass in solution is probably not uniform in time. However, the data shown in Figure 4 are insufficient to identify any trends in estimation variance. If, for practical purposes, the variance is assumed uniform in time such that a standard method of moments estimator can be used, the coefficient of variation of the bromide mass estimate is 0.20. This appears quite satisfactory, given the observed sensitivity of the estimated mass in solution to sampling density.

The average observed mass is 0.41 kg less than the estimated mass injected. This difference, the bias, is probably significant. A conventional t test is not strictly applicable in this case because of the nonuniform variance. However, if used as a rough measure, this test would judge the difference significant with confidence of about 0.95. Factors potentially contributing to moment estimation bias include (1) bias in point concentrations introduced by the sampling and analytical procedures, (2) consistent over- or underestimation by the quadrature procedure used to approximate (1), (3) consistent errors introduced by the assumption of a spatially uniform porosity field, and (4) a biased estimate of the mean porosity. Quantitative assessment of the first two of these factors is analytically intractable and not addressed here. The assumption of spatial uniformity in the porosity field will contribute to the estimation bias if the porosity and concentration fields are correlated. Unfortunately, it was experimentally infeasible to collect the data required to identify such a correlation.

The mean porosity estimate is, of course, subject to uncertainty. As was noted earlier, because of the difficulty in obtaining undisturbed samples from depth in the aquifer, relatively few data are available to evaluate the mean porosity estimate. However, it should be noted that eliminating the bias observed in Figure 4 would require an increase in the mean porosity from 0.33 to 0.37. Such a difference cannot be explained by the variability in the measured values used to estimate the mean. However, earlier estimates of the mean porosity near the site have been as large as 0.38 [*Sudicky et al.*, 1983].

Figure 5 compares the mass estimates for chloride and bromide when each is normalized by the appropriate estimated injected mass. Paired estimates are shown for all sampling sessions but the last. Only bromide data are available for the last session because significant interference between the experimental plumes and the underlying landfill plume invalidated chloride observations. Different analysts working independently of each other prepared the data for the two tracers. Since the normalized point observations of chloride and bromide concentrations are nearly indistinguishable throughout the experiment, the data in Figure 5 provide an opportunity to assess the stability of the estimation process. While individual mass estimates do differ somewhat, particularly those for 381 and 429 days after injection, the differences show no distinct pattern or trend, and average values over time are almost identical. The average relative mass and coefficient of variation for chloride are 0.90 and 0.16, while the same parameters for bromide are 0.89 and 0.20. The bias and variability for bromide are just slightly greater than for chloride.

CENTER OF MASS AND ADVECTION

The estimated coordinates of the centers of mass of the bromide and chloride plumes for each synoptic sampling session are tabulated in Table 3. The coordinates are given in the field coordinate system shown in Figure 5 of *Mackay et al.* [this issue]. As was discussed previously, only data for bromide are available for the last sampling session. Note that because the concentration distribution can be multimodal and asymmetric, the center of mass may not coincide with the location of the highest point or vertically averaged concentration.

Horizontal Trajectory

Figure 6 presents graphically the horizontal trajectory of the centers of mass of the two plumes. Individual locations for the two tracers are essentially indistinguishable, indicating that little estimation variability is introduced by sampling and measurement noise or by differences in smoothing that could have been introduced by the two analysts who independently carried out the calculations.

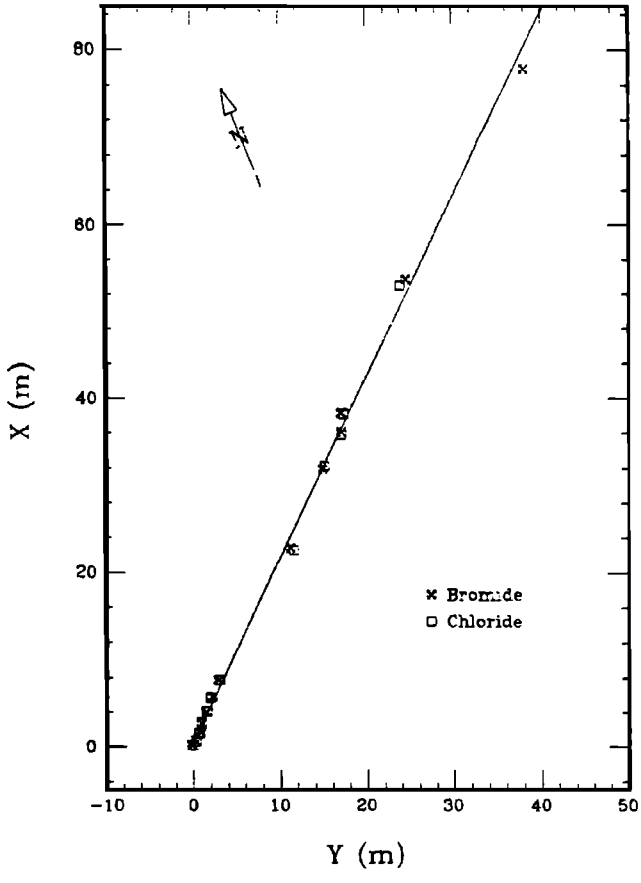

Fig. 6. Horizontal trajectories of the centers of mass of the chloride and bromide plumes.

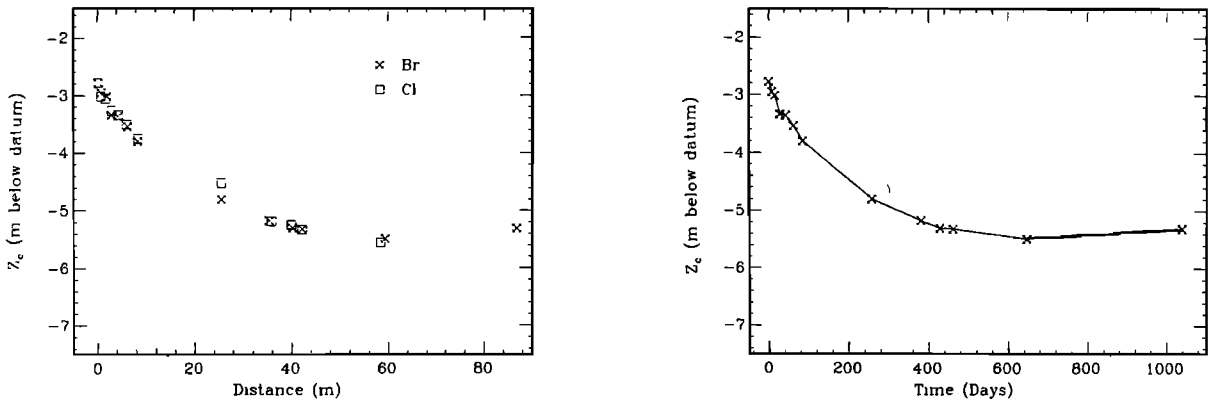

Fig. 7. Vertical displacement of the centers of mass of the chloride and bromide plumes. (left) Vertical location of the center of mass for each plume as a function of horizontal displacement along the linear trajectory shown in Figure 6. (right) Average vertical coordinate of the centers of mass of the bromide and chloride plumes as a function of time. Straight line segments connect the points.

The data of Figure 6 suggest that the tracer plumes followed a remarkably linear horizontal trajectory over the duration of the experiment. The hydraulic gradient at the site is known to undergo small seasonal changes in direction (see, for example, Figure 3 of *Mackay et al.* [this issue]). However, the effects of this temporal variability are apparently small and undetectable in the center of mass data, at least for the available temporal resolution and estimation uncertainty. Shown on Figure 6 is the straight line which minimizes the sum of the squared orthogonal distances between the data points and the line (the least normal squares line; compare *Hirsch and Gilroy* [1984]). The fit to this line is excellent. The largest deviation, occurring for the last sampling session, is 1.56 m. This deviation could indicate a small deflection in the trajectory over the last year of the experiment. However, it is inappropriate to reject the hypothesis of linearity, since the estimation standard deviation for the center of mass location, although not quantified, is probably no smaller than 1.5 m.

The best fit horizontal trajectory is directed 25.5° clockwise from the x axis, or N47.5°E. This direction is in the center of the range observed for the direction of the hydraulic gradient and is within 2° of the estimated temporal mean direction (see Table 2). This suggests that horizontal anisotropy in the mean hydraulic conductivity field is very small to negligible. *Sudicky* [this issue] reaches the same conclusion via an analysis of laboratory measured hydraulic conductivities from 1279 core samples taken adjacent to the monitored zone.

Vertical Displacement

The vertical coordinate of the center of mass for each sampling session and each tracer is estimated in a manner exactly analogous to that described earlier for the horizontal moments. The only difference is that in this case C_z of (9) is defined as

$$C_z(x, y, t) = \int_{-\infty}^{\infty} C(x, y, z, t)\, z\, dz \qquad (11)$$

The vertical center of mass coordinates estimated in this manner have been found to be very insensitive to the smoothing induced by the horizontal quadrature technique.

Figure 7 depicts the vertical displacement of the center of mass of the tracer plumes. Figure 7*a* presents the vertical locations of the centers of mass of both the bromide and chloride plumes as functions of horizontal displacement. Horizontal displacement distances are determined by orthogonal projection of the individual data points onto the linear trajectory shown in Figure 6. Figure 7*b* shows the average value of the estimated vertical coordinate for the two tracers as a function of elapsed time. The data points are connected by straight lines to help visualize changes in slope. Note that $z = 0$ represents ground elevation at the injection wells and that the injection wells are screened over the interval $z = -2.1$ to $z = -3.7$ m.

The total vertical displacement over the duration of the experiment is small, about 2.7 m over 1038 days. As a component of the total displacement the vertical motion is negligible. However, Figure 7 reveals that in contrast to the horizontal trajectory, the vertical trajectory is not uniform over time and space. All of the vertical displacement occurs over the first 650 days of transport, with the center of mass actually rising slightly over the last 390 days. The vertical trajectory is generally concave upward, indicating that the downward vertical velocity is decreasing with time. Note that with relatively small changes in magnitude (<0.1 m) for a few points the trajectory would appear smoothly concave upward over its entire length. Such differences are probably within the estimation error for the vertical coordinate.

Sudicky et al. [1983] observed a small vertical displacement, about 0.8 m over 121 days, during their natural gradient tracer experiment at a neighboring site. From Figure 7, the vertical displacement for the first 120 days of the current experiment is estimated as about 1 m. Thus the results from the two experiments are reasonably consistent. Sudicky et al. concluded that the vertical velocity component was an order of magnitude less than the horizontal. They attributed the vertical displacement to hydraulic head differences and the density contrast between their plume and the native groundwater.

While the reason(s) for the nature and magnitude of the observed vertical movement shown in Figure 7 are not fully understood at this time, it is likely that a number of mechanisms are jointly responsible. These include a small vertical component in the regional velocity field, the density contrast between the plume and the native groundwater, local infiltration and recharge, and (at later times) interaction with the underlying, denser landfill plume.

Solute Velocity

The mean solute velocity at the plume scale U may be investigated by examining the slope of the center of mass dis-

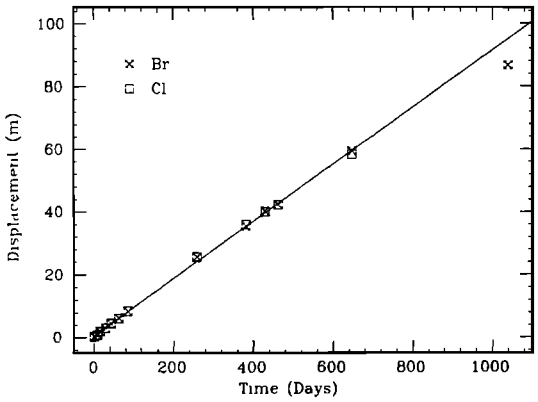

Fig. 8. Horizontal displacement of the centers of mass of the chloride and bromide plumes along the linear trajectory of Figure 6 as a function of time since injection.

placement versus time relationship. As was noted in the previous section, the contribution of the vertical component to the total displacement is negligible, so attention here will be focused on the horizontal displacement. Figure 8 plots the horizontal displacement along the linear trajectory shown in Figure 6 against travel time for the two tracers. As before, the horizontal displacement distances are determined by orthogonal projection of the individual data points onto the trajectory. Not surprisingly, values for the two tracers are practically indistinguishable.

The data in Figure 8 for the first 650 days of transport plot as a strikingly linear function of time. Shown on the figure is the ordinary least squares linear fit to these data. Evidently, the mean velocity field for this time period and this portion of the aquifer is well modeled as spatially and temporally uniform. The extent of the plume appears to have been large enough (vertically about 20 times the vertical correlation scale of the hydraulic conductivity, and horizontally from 2.3 to 30 times the horizontal correlation scale) that local variations in the velocity field did not dominate the average movement of the plume as a whole. Any large-scale temporal changes in the velocity field, such as might be induced by seasonal changes in mounding below the upgradient landfill, were either very small and/or could not be resolved by the relatively low frequency of sampling over time.

The magnitude of the mean velocity determined from the linear fit in Figure 8 is 0.091 m/day. *Mackay et al.* [this issue] show that this value is reasonably consistent with predictions using the data on hydraulic gradient, conductivity, and porosity given in Table 2 (see also *Sudicky* [this issue]). It also falls in the interval between the mean velocity estimates for the "fast" (0.25 m/day) and "slow" (0.071 m/day) zones observed during the earlier experiment at a neighboring site [*Sudicky et al.*, 1983].

The displacement for the last sampling session clearly deviates from the linear relationship defined by the first 12 sampling dates. The plume appears to have decelerated somewhat in the time between the last two samplings, such that the center of mass is nearly 9 m behind its predicted location based on the previous observations. Recall that this sampling session also exhibited the largest deviation from the fitted linear trajectory.

Figure 3, discussed earlier, provides a possible explanation for this behavior. While the tracer distribution always exhibited an upstream dip and was bimodal to some extent since at least the 85th day, the plume on the last sampling date had become distinctly bimodal and vertically separated into two layers. Note that the center of mass of the downgradient lobe (upper layer) is about 13 m beyond the center of mass of the plume as a whole (see Table 3). If plotted on Figure 8 this point would be about 4 m above the best fit line, which is probably a statistically significant deviation. This suggests that by the last sampling date, the plume had encountered a region of the aquifer with a relatively large-scale inhomogeneity in its velocity field. The plume scale mean velocity became in effect an average over two zones: an upper zone with a mean velocity somewhat greater than the observed plume average over the previous two years, and a lower zone with a mean velocity less than the observed plume average. By the last year, most of the mass had accumulated in the lower zone so that it dominated the solute motion averaged over the entire plume. The result is that the plume as a whole appears to have slowed.

Spatial Covariance and Dispersion

As was described in an earlier section, the spatial covariance structure of a concentration distribution provides a measure of the spread of the distribution about its center of mass. Changes in the covariance structure over time (or space) reflect, but do not necessarily completely characterize, the changes in the concentration distribution that occur because of heterogeneity in the solute velocity field. Here, we focus on the horizontal components of the spatial covariance tensor. The experimental data reveal that the vertical thickness of the tracer plumes remained essentially unchanged over the duration of the experiment (see Figure 9 of *Mackay et al.* [this issue]). Also, although changes in the internal vertical structure of the plumes can be observed on plots such as those shown in Figure 9 of *Mackay et al.* [this issue], sampling variability of the components of the covariance tensor involving the vertical direction is large. In general, temporal variation in estimates of the vertical components of the spatial covariance tensor cannot be distinguished from sampling noise. Therefore in this paper only the purely horizontal components are examined.

Table 3 lists the horizontal components of the estimated spatial covariance tensor for both bromide and chloride. To facilitate the discussion, the components are given in a rotated coordinate system (x', y'). The x' direction is parallel to the linear horizontal trajectory (and therefore to the estimated mean velocity vector), and the y' direction is perpendicular to the trajectory. Defined in this manner, x' and y' correspond to

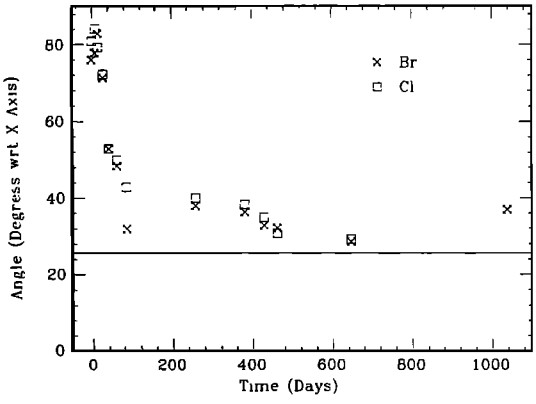

Fig. 9. Angle between the major principal axis of the estimated spatial covariance tensor and the x axis as a function of time. Angles are measured as clockwise rotations from the x axis. Solid line indicates the angle between the estimated mean velocity vector and the x axis (25.5°).

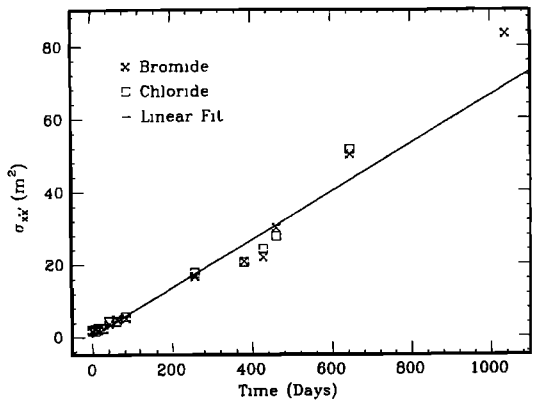

Fig. 10*a*.

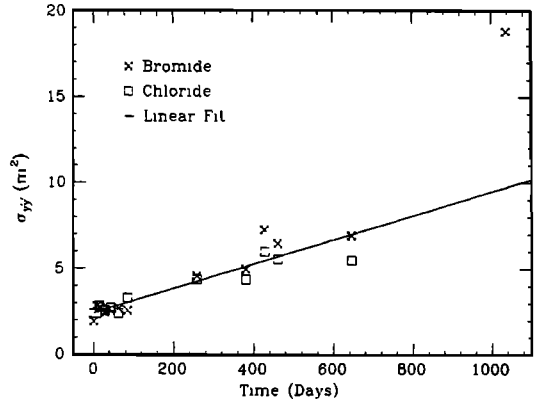

Fig. 10*b*.

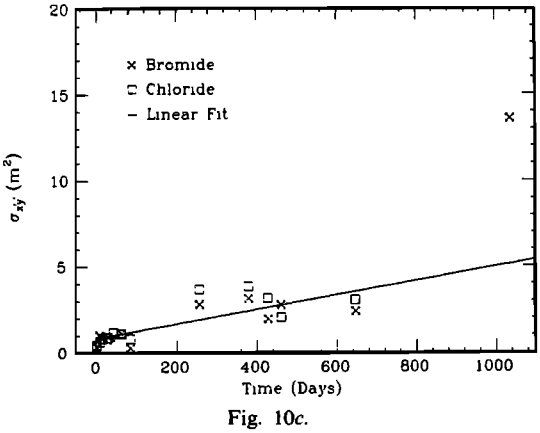

Fig. 10*c*.

Fig. 10. Components of the estimated spatial covariance tensor of chloride and bromide as functions of time. Coordinate system is aligned with the estimated mean velocity vector, with x' parallel and y' perpendicular to the velocity, respectively. (*a*) Longitudinal variance $\sigma_{x'x'}$. (*b*) Transverse variance $\sigma_{y'y'}$. (*c*) Covariance $\sigma_{x'y'}$.

the longitudinal and transverse directions of traditional advection-dispersion terminology. The components are estimated using the field coordinate system and then rotated 25.5° clockwise using the standard cartesian tensor rotational transformation [compare *Jeffreys*, 1974].

As was described earlier, in plan view the initial pulse of tracer was somewhat rectangular in shape, with its long side parallel to the field y axis (see Figure 8 of *Mackay et al.* [this issue]). Over time, the plume evolved into an elongated shape, with its major axis roughly aligned with the direction of the plume's mean motion. The data of Table 3 help to quantify this observed behavior. For the first 4 sampling sessions the estimated $y'y'$ components of the covariance tensor are larger than the $x'x'$ components, reflecting the plume's greater dimension in the transverse direction than in the longitudinal direction. From the fifth sampling session on, the $x'x'$ term is larger than the $y'y'$ term and the difference between the two terms increases over time as the plume becomes more and more elongated in the longitudinal direction.

Figure 9 graphically depicts this aspect of the plume behavior. Shown there is the angle between the field x axis and the major (longer) principal axis of the estimated covariance tensor as a function of time. The solid line corresponds to the angle of rotation of the estimated mean velocity (25.5°). Recall that the principal axes of a tensor are defined by the rotation required to diagonalize the tensor. For an ellipsoidal distribution the principal axes correspond to the major and minor axes of the ellipsoid. In the context of the analysis here, the principal axes may also be interpreted as the major and minor axes of a multivariate Gaussian distribution fitted to the observed concentration distribution. While the data in Figure 9 show some scatter between tracers, the trend over time is clear. Initially, when the plume is oriented roughly symmetrically about the field coordinate directions and is wider than it is long, the major principal axis is rotated nearly 90° (clockwise) from the x axis. In other words, the major principal axis is nearly parallel to the y axis. With passing time the angle decreases as the plume becomes oriented with and elongated in the direction of mean motion. It is interesting to note that the major principal axis never becomes fully aligned with the mean velocity vector. However, the direction of the major principal axis does appear to approach the direction of the velocity vector nearly monotonically over the first 647 days of travel time. The last sampling session then shows an increased difference between the two directions. While this may be attributable to sampling variability, it may also be a manifestation of the inhomogeneity in the mean velocity field which caused the plume to decelerate and split into two layers over the last year of the experiment.

Figure 10 presents plots showing the three estimated horizontal components of the spatial covariance tensor (in the rotated coordinate system aligned with the mean velocity vector) as functions of time since injection. Figure 10*a* presents the data for $\sigma_{x'x'}$, Figure 10*b* shows $\sigma_{y'y'}$, and Figure 10*c* shows $\sigma_{x'y'}$. Note that the ordinate scale is not the same for all three plots. Estimates for both chloride and bromide are included. The scatter between the data for the two tracers is greater than that observed for the locations of the centers of mass (see Figure 8), as expected, since the sensitivity of the estimation methodology increases with the order of the moment. However, in an absolute sense the sensitivity of the covariance estimates to the particular tracer remains small, especially for the longitudinal component.

Perhaps the simplest and most naive model that would in practice be hypothesized to describe the experimental plume movement is the classic advection-dispersion equation with constant effective coefficients (mean velocity and apparent dispersivity). Under those conditions, (5) is valid with constant D. A linear relationship is then expected between the magnitudes of the components of the covariance tensor and time. Shown on each of the plots in Figure 10 are the ordinary least squares linear fits to all the data points but the last. The last sampling session is excluded because the mean velocity field did not remain homogeneous over the last year of the experiment. Although the data do not conclusively rule out the possibility of linear relationships for each of the plots, the residuals from

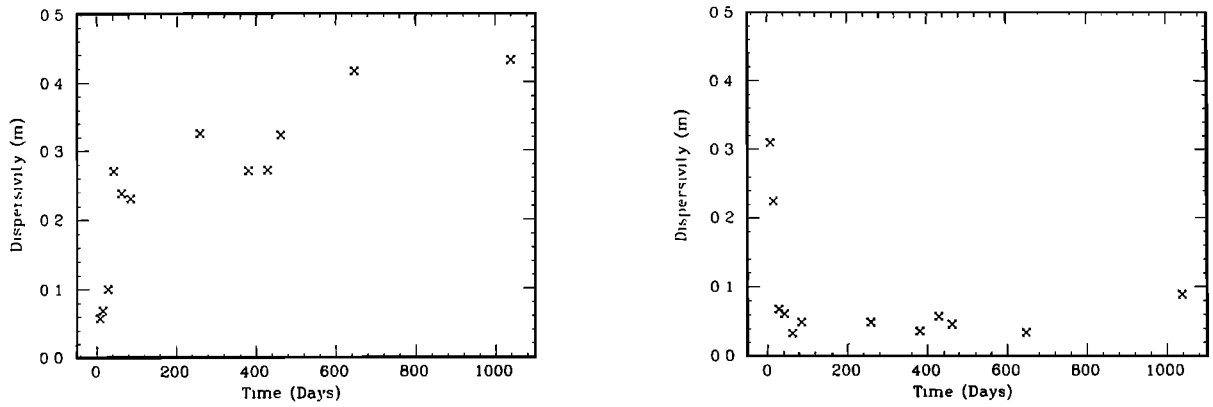

Fig. 11. Estimated apparent dispersivities implied by the assumption of a linear growth in the covariance over the time interval (1, t). Average values for the two tracers are shown. (left) Longitudinal dispersivity $A_{x'x'}$. (right) Horizontal transverse dispersivity $A_{y'y'}$.

the fitted lines indicate that nonlinear relationships may be more satisfactory. In particular, the longitudinal component residuals suggest an upward curvature to the data, and the transverse and cross component residuals suggest downward curvature. It appears that the rate of growth of the spatial covariance components over the first 650 days of transport (during which the mean velocity was constant) was nonuniform, contrary to the classic constant-coefficient model.

For purposes of later comparison, apparent dispersivities may be calculated from the slopes of the lines in Figure 10 using (7):

$$A_{x'x'} = 0.36 \text{ m} \qquad A_{y'y'} = 0.039 \text{ m} \qquad A_{x'y'} = 0.023 \text{ m}$$

Such fitted dispersivities represent average values over the first 647 days of displacement. Predictions of second moment behavior using these average values in the advection-dispersion equation would be unsatisfactory, particularly if the observed distribution for the first sampling session is used as the initial condition. In addition, such predictions would of course be unable to reproduce the bimodal internal structure of the plumes.

Another approach commonly used to analyze the dispersive behavior of solute plumes is sequential calibration. A solution to the advection-dispersion equation for constant, spatially uniform parameters is calibrated to the observations from each sampling session. The resulting set of calibrated values of dispersivity is then examined as a function of travel time or, equivalently, displacement. Such analyses formed the basis for many of the early discussions of "scale-dependent" dispersion [i.e., *Anderson*, 1979; *Sudicky et al.*, 1983].

Figure 11 presents a similar analysis for the data from this experiment. Shown there are the functions

$$A_{x'x'}(t) = \frac{1}{2|\mathbf{U}|} \frac{\sigma_{x'x'}(t) - \sigma_{x'x'}(1)}{t - 1} \qquad A_{y'y'}(t) = \frac{1}{2|\mathbf{U}|} \frac{\sigma_{y'y'}(t) - \sigma_{y'y'}(1)}{t - 1}$$

where the values of $\sigma_{x'x'}(t)$ and $\sigma_{y'y'}(t)$ are taken from Table 3, and the first sampling session ($t = 1$ day) is chosen as the initial condition. For clarity, average values for the two tracers are shown. Figure 11*a* shows $A_{x'x'}(t)$, and Figure 11*b* shows $A_{y'y'}(t)$. Comparison with (7) reveals that $A_{x'x'}(t)$ and $A_{y'y'}(t)$ are analogs of the calibrated dispersivities described in the previous paragraph. They are the apparent dispersivities implied (from equation (7)) by the assumption of a linear growth in the covariance over the time interval (1, t). While the data points in Figure 11 show some scatter, several patterns emerge. The experimental data exhibit a scale-dependent dispersive behavior in the longitudinal direction (Figure 11*a*) quite similar to that observed in previous calibration studies. The value of $A_{x'x'}$ increases from 0.06 to 0.43 m over the duration of the experiment. Note that this range brackets the average linear-fit value of 0.36 m discussed above. The transverse apparent dispersivity, shown in Figure 11*b*, is dominated by sampling noise at early times, but shows no significant increase in magnitude analogous to the behavior of the longitudinal apparent dispersivity. Its value remains in the vicinity of the average linear-fit value.

The apparent dispersivities in the previous paragraphs are in the lower ends of the range of values for field-scale apparent dispersivities reported in the literature [compare *Anderson*, 1979; *Gelhar et al.*, 1985]. The longitudinal dispersivity values are somewhat larger than those reported by *Sudicky et al.* [1983] for the previous 121-day experiment near the site, while the transverse dispersivities are comparable.

Several recent stochastic transport studies have investigated the behavior of the ensemble covariance as a function of time for spatially variable pore water velocity fields. Of particular interest here is the study of *Dagan* [1982, 1984]. Using a linearized, first-order approximation and an isotropic exponential covariance function for the logarithm of hydraulic conductivity (ln K), Dagan found expressions for the time dependence of the components of the covariance tensor for both two- and three-dimensional steady flow in an infinite aquifer. Because the estimated exponential covariance function of ln K for the Borden aquifer shows distinct vertical anisotropy (see Table 2 and *Sudicky* [this issue]), and because the vertical extent of the experimental plume is at least 20 times the estimated vertical correlation scale, the two-dimensional form is examined here as the most appropriate approximation to conditions at the experimental site. For this case, Dagan has found (G. Dagan, personal communication, 1986):

$$\sigma_{x'x'}(t) = 0.74\sigma_{\ln K}{}^2 l_{\ln K}{}^2 \left\{ 2\frac{t}{T} + \frac{3}{2} + 3\left[Ei\left(-\frac{t}{T}\right) - \ln\left(\frac{t}{T}\right) - \gamma \right] + 3\,\frac{e^{-t/T}\left[1 + \frac{t}{T}\right] - 1}{[t/T]^2} \right\} \tag{12}$$

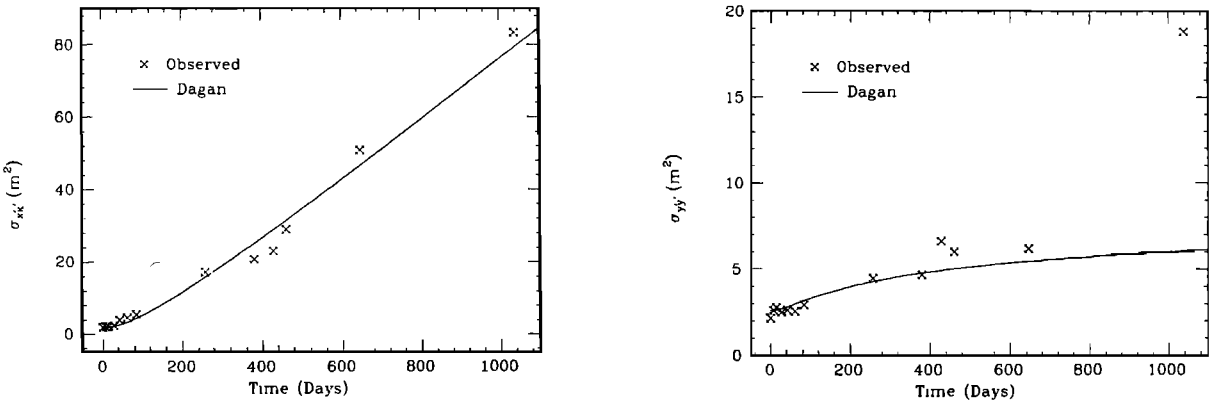

Fig. 12. Comparison of estimated longitudinal and transverse components of the spatial covariance tensor with the theoretical results of *Dagan* [1984] for $\sigma_{\ln K}^2 = 0.24$, $l_{\ln K} = 2.7$ m, and $|U| = 0.091$ m/day. (left) Longitudinal component. (right) Transverse component.

$$\sigma_{y'y'}(t) = 0.74\sigma_{\ln K}^2 l_{\ln K}^2 \left\{ -\frac{3}{2} - \left[Ei\left(-\frac{t}{T}\right) - \ln\left(\frac{t}{T}\right) - \gamma \right] - 3\,\frac{e^{-t/T}\left[1+\frac{t}{T}\right]-1}{[t/T]^2} \right\} \tag{13}$$

$$\sigma_{x'y'}(t) = 0 \tag{14}$$

where $\sigma_{\ln K}^2$ is the variance of $\ln K$; $l_{\ln K}$ is the correlation scale of the $\ln K$ covariance function; $\gamma = 0.5772\cdots$ is Euler's constant; $Ei(-t)$ is the exponential integral; and $T = l_{\ln K}/|U|$ is a characteristic time. Equations (12)–(14) differ from previously published results [*Dagan*, 1982, 1984] only by correction of a typographical error and addition of the leading coefficient, which arises from the vertical integration required for valid comparison with the experimental spatial moments. Recall that x' and y' are defined as parallel and perpendicular to the mean velocity vector, respectively. Note that (12)–(14) assume that $\sigma_{x'x'}(0) = \sigma_{y'y'}(0) = \sigma_{x'y'}(0) = 0$. For nonzero initial covariances (12)–(14) must be augmented by the appropriate initial values.

Figure 12 presents the results of calibrating the functions given in (12) and (13) to the experimental data of Figures 10*a* and 10*b*. Values of $\sigma_{\ln K}^2$ and $l_{\ln K}$ have been chosen to provide a visual best fit with the data, assuming $|U| = 0.091$ m/day, $\sigma_{x'x'}(0) = 1.8$ m^2, and $\sigma_{y'y'}(0) = 2.6$ m^2. For clarity, only average values of the experimental data for the two tracers are shown. Figure 12*a* shows the longitudinal component, and Figure 12*b* shows the transverse component.

The calibrated parameter values are

$$\sigma_{\ln K}^2 = 0.24 \qquad l_{\ln K} = 2.7 \text{ m}$$

These values compare reasonably well with the independent estimates of these parameters presented by *Sudicky* [this issue] and summarized in Table 2. The two correlation scale estimates are essentially the same, while the calibrated $\ln K$ variance is somewhat less than the value measured by Sudicky. The fit between the data and the theoretical curves is quite satisfactory, particularly since the theoretical curves are ensemble expectations, and is superior to the linear fits of Figure 10. The variation over time and the relative magnitudes of the two components are well reproduced by the theory. The last sampling point does show a significant departure from the trend of the data as well as from the calibrated curve for the transverse term; however, the validity of the comparison for this data point is questionable because of the change in mean velocity and internal structure of the plume discussed in detail earlier.

Theoretical expressions for the apparent longitudinal and transverse dispersivity may be obtained by differentiation of (12) and (13) and application of (7). Of special interest to many investigators has been the limiting value of dispersivity for large values of time (see, especially, *Gelhar and Axness* [1983]). For this case (12) and (13) yield

$$A_{x'x'}(t) \to \sigma_{\ln K}^2 l_{\ln K} \qquad t \to \infty \tag{15}$$

$$A_{y'y'}(t) \to 0 \qquad t \to \infty \tag{16}$$

Substitution of the calibrated parameter values results in the estimate

$$A_{x'x'}(t) \to 0.49 \text{ m} \qquad t \to \infty$$

Note from Figures 11 and 12 that these limiting values appear reasonably consistent with the observed behavior prior to the last sampling session. The limiting value of the longitudinal dispersivity is somewhat larger than values estimated by assuming an overall linear fit (Figure 10) or by assuming linearity prior to each sampling session (Figure 11). Of particular interest is the significant slowing in the growth of the transverse variance over the period from 300 to 650 days after injection, suggesting that a small or zero asymptotic value would not be inappropriate for the transverse dispersivity if the velocity field were to remain statistically homogeneous. As was noted earlier, the last sampling session exhibited the effects of a significant inhomogeneity in the mean velocity field, which invalidates extension of the theoretical results beyond 647 days.

In summary, the time-dependent behavior of the estimated spatial covariance tensor over the first 647 days is reasonably well described by the theoretical model of *Dagan* [1984], even though the assumptions underlying the Dagan model are only approximately satisfied at the experimental site. The relative magnitudes of the diagonal components of the tensor are well matched using calibrated values of the parameters of the $\ln K$ distribution that agree well with independent measurements. The predicted asymptotic values of these components using the calibrated parameters appear reasonable. The off-diagonal component of the covariance shows some growth during the early phase of the experiment, contrary to theory, but stabilizes at a small value.

The fitted theoretical curves in Figure 12 suggest that asymptotic conditions had not been reached after 647 days of transport through a homogeneous mean velocity field. However, sometime after 647 days the tracers appear to have encountered a large-scale heterogeneity in the velocity field that resulted in a reduction in the mean solute velocity and a large increase in the transverse and off-diagonal components of the covariance tensor. The extent to which this heterogeneity would be smoothed over time is of course unknown. However, because of its scale, its impact is not well represented by the stochastic structure assumed in the Dagan model.

SUMMARY OF THE STUDY AND RESULTS

The data base from the large-scale natural gradient field experiment on groundwater solute transport described in the work by *Mackay et al.* [this issue] has provided an opportunity to examine the three-dimensional movement of a tracer plume in considerable detail. Synoptic sampling of a dense network of multilevel samplers yielded a large set of point measurements for which plume movement and structure can be studied with a relatively high degree of certainty. The aquifer material at the experimental site exhibits enough spatial variability in its hydraulic properties that the effects can be detected and investigated. Yet the variability is small enough that relatively simple models of spatial variability appear applicable and long-term effects are observable.

Because of the expected variability in point concentrations due to both spatial variability in the pore water velocity field and measurement noise, we have focused our analysis on the zeroth-, first-, and second-order spatial moments, integrated measures defined over the volume of a plume. While the lower-order moments cannot fully characterize the structure of a solute plume, they do provide measures of the mass, mean velocity, and dispersion. We have developed moment estimators using quadrature approximations tailored to the density of the sampling network. These estimators appear to be robust with acceptable sampling variability, although no formal studies of the sampling properties are available.

The zeroth-order spatial moment measures the mass of dissolved solute. Estimates of the mass for both bromide and chloride are somewhat smaller than the injected mass, but are relatively uniform over time (Figures 4 and 5). Loss of mass because of dilution below background or sample extraction cannot be detected.

The first-order spatial moments measure the location and movement of the center of mass of the solute plume. Analysis of the first-order moment estimates indicates that the experimental tracer plumes traveled along identical trajectories. The horizontal trajectory is linear and at an angle of 25.5° with respect to the field coordinate system and the a priori assumed direction of the hydraulic gradient (Figure 8). Subsequent analysis has shown the trajectory to be nearly aligned with the hydraulic gradient. The vertical displacement is small, but the vertical trajectory is curvilinear, concave upward (Figure 7). The vertical component of the mean solute velocity vector is negligible.

The estimated mean solute velocity is also identical for both tracers and is spatially and temporally uniform for the first 647 days of residence time (Figure 8). Its magnitude is 0.091 m/day. In the third year of transport, the plumes apparently encountered a relatively large-scale heterogeneity in the velocity field, leading to a distinct vertical layering, with the upper layer traveling at a higher velocity than the lower (Figure 3). The rate of advance of the center of mass of the plume as a whole slowed.

The second-order spatial moments define the spatial covariance tensor, which measures the spread of a plume about its center of mass. Here we have focused on the horizontal components of the covariance tensor, because vertical spreading was negligible and changes in the estimated vertical components over time cannot be distinguished from estimation variability.

The estimated horizontal components of the covariance tensor evolve over time in a manner consistent with the qualitative shape changes observed from plots of the concentration data. The major principal axis, initially nearly aligned with the y axis, rotates smoothly over time until it is nearly aligned with the mean solute velocity vector, as the plume itself elongates and orients its long axis with the direction of movement (Figure 9).

Plots of the components of the covariance tensor as functions of time show evidence of what is commonly called scale-dependent dispersion (Figures 10 and 11). The rate of growth of the covariance over time is probably not linear, as would be predicted by the classic advection-dispersion equation with constant effective parameters. The theoretical results of *Dagan* [1984] calibrate well to the estimated covariance data for the first 647 days of transport (Figure 12). The calibrated values of the parameters, $\sigma_{\ln K}^2 = 0.24$ and $I_{\ln K} = 2.7$ m, satisfactorily match the independently measured values obtained by *Sudicky* [this issue]. The asymptotic longitudinal dispersivity obtained from the calibration is 0.49 m. The estimated covariance terms for the last sampling session, 1038 days after injection, are inconsistent with the earlier data and with the Dagan model, particularly for the transverse and off-diagonal components. This behavior is probably attributable to the observed heterogeneity in the velocity field described above.

DISCUSSION

A number of different approaches to the analysis of the data base from the experiment described in the work by *Mackay et al.* [this issue] are possible. Here, hoping to develop information useful for the testing and validation of mathematical transport models, we have deliberately chosen to focus on the lower-order spatial moments of the concentration distribution. The moments themselves are defined independently of any model of the physics (or chemistry) of transport at the site. Furthermore, estimation of the moments from point observations requires few model assumptions, and this study has shown that the estimators are quite insensitive to those few assumptions.

After estimation, physically based models, such as the classic advection-dispersion equation with constant coefficients or the stochastic models of *Dagan* [1984] or *Gelhar and Axness* [1983], are, of course, required to interpret moment behavior over time and space. The predictive ability of such models may be explored using the independently determined measures of plume movement and structure provided by moment estimates. Spatial moments are particularly well suited to the investigation of stochastic models, because stochastic model predictions are necessarily expressed as expectations (over the ensemble). For the single realization provided by the experimental observations, integrated measures are appropriate tools for comparison and analysis.

In this study we have shown that the stochastic transport model of *Dagan* [1984] calibrates well to the moment esti-

mates over the duration of the experiment for which the assumptions of the model are appropriate. The calibration is satisfactory in terms of both the functional form of the covariance versus time relationship as well as the calibrated values of the two parameters of the ln K distribution. Calibration of the classic model with constant coefficients is less satisfactory.

We have not addressed the much more difficult problem of model validation. However, in a companion paper *Sudicky* [this issue] shows that independent prediction of the moment behavior using measured characteristics of the ln K distribution and the models of *Dagan* [1984] and *Gelhar and Axness* [1983] is quite good over the duration of the experiment for which the model's assumptions appear adequate.

There remain many unanswered questions in the application and testing of sophisticated transport models. *Sposito et al.* [1986] discuss a number of these. The relationship between ensemble behavior and transport in a given aquifer (a single realization) is of particular interest in experimental studies. An equally important issue is our ability to describe aquifer heterogeneity with relatively simple statistical models. The behavior of the experimental plume in the third year of transport demonstrates some of the difficulties. The heterogeneity in the velocity field that led to the bifurcation of the plume at 1038 days appears to have been at a large enough scale that it is not well represented by the statistically homogeneous model of variability that proved satisfactory for the earlier phase of transport. However, the scale at which this heterogeneity might be treated as random is clearly very large, so large that ergodicity requirements would probably be very difficult to meet [compare *Dagan*, 1984]. A more sophisticated model of aquifer variability, perhaps incorporating nonstationarity, appears necessary. Hopefully, the experimental data base will prove helpful in such future work.

Acknowledgments. The work reported here was supported by the R. S. Kerr Environmental Research Laboratory of the U.S. Environmental Protection Agency (CR-808851) and by the National Science Foundation (ECE 84-51565). It has not been subjected to the Environmental Protection Agency's required peer and administrative review and therefore does not necessarily reflect the views of that Agency and no official endorsement should be inferred. I acknowledge the invaluable contributions of a number of colleagues: T. C. Black and P. J. Fennessy assisted in the design and coded the moment estimation routines; A. Y. Chen, J. W. Davis, and K. K. Murphy maintained the data base and developed the necessary data management routines; and D. J. Knight assisted in the reduction of the bromide data. I am also grateful for discussions with G. Dagan, L. Gelhar, D. Mackay, P. Roberts, and E. Sudicky, which influenced the direction of this work.

REFERENCES

Abramowitz, M., and I. A. Stegun (Eds.), *Handbook of Mathematical Functions, App. Math. Ser. 55*, National Bureau of Standards, Washington, D. C., 1970.

Anderson, M. P., Using models to simulate the movement of contaminants through groundwater flow systems, *CRC Crit. Rev. Environ. Control, 9*, 97–156, 1979.

Aris, R., On the dispersion of a solute in a fluid flowing through a tube, *Proc. R. Soc. London, Ser. A, 235*, 67–78, 1956.

Bear, J., *Dynamics of Fluids in Porous Media*, Elsevier, New York, 1972.

Cussler, E. L., *Diffusion: Mass Transfer in Fluid Systems*, Cambridge University Press, New York, 1984.

Dagan, G., Stochastic modeling of groundwater flow by unconditional and conditional probabilities, 2, The solute transport, *Water Resour. Res., 18*(4), 835–848, 1982.

Dagan, G., Solute transport in heterogeneous porous formations, *J. Fluid Mech., 145*, 151–177, 1984.

Gelhar, L. W., and C. L. Axness, Three-dimensional stochastic analysis of macrodispersion in aquifers, *Water Resour. Res., 19*(1), 161–180, 1983.

Gelhar, L. W., A. L. Gutjahr, and R. L. Naff, Stochastic analysis of macrodispersion in a stratified aquifer, *Water Resour. Res., 15*(6), 1387–1397, 1979.

Gelhar, L. W., A. Mantoglou, C. Welty, and K. R. Rehfeldt, A review of field-scale physical solute transport processes in saturated and unsaturated porous media, *Final Proj. Rep. EPRI EA-4190*, Elec. Power Res. Inst., Palo Alto, Calif., 1985.

Güven, O., F. J. Molz, and J. G. Melville, An analysis dispersion in a stratified aquifer, *Water Resour. Res., 20*(10), 1337–1354, 1984.

Hirsch, R. M., and E. J. Gilroy, Methods of fitting a straight line to data: Examples in water resources, *Water Resour. Bull., 20*(5), 705–719, 1984.

Jeffreys, H., *Cartesian Tensors*, Cambridge University Press, New York, 1974.

MacFarlane, D. S., J. A. Cherry, R. W. Gillham, and E. A. Sudicky, Migration of contaminants in groundwater at a landfill: A case study, 1, Groundwater flow and plume delineation, *J. Hydrol., 63*, 1-29, 1983.

Mackay, D. M., D. L. Freyberg, P. V. Roberts, and J. A. Cherry, A natural gradient experiment on solute transport in a sand aquifer, 1, Approach and overview of plume movement, *Water Resour. Res.*, this issue.

Matheron, G., and G. deMarsily, Is transport in porous media always diffusive? A counterexample, *Water Resour. Res., 16*(5), 901–917, 1980.

Morrison, D. F., *Multivariate Statistical Methods*, 2nd ed., McGraw-Hill, New York, 1976.

Nwankwor, G. I., J. A. Cherry, and R. W. Gillham, A comparative study of specific yield determinations for a shallow sand aquifer, *Ground Water, 22*(6), 764–772, 1984.

Roberts, P. V., M. N. Goltz, and D. M. Mackay, A natural gradient experiment on solute transport in a sand aquifer, 3, Retardation estimates and mass balances for organic solutes, *Water Resour. Res.*, this issue.

Sampson, R. J., SURFACE II graphics system, revision one, 240 pp., Kans. Geol. Surv., Lawrence, 1978.

Simmons, C. S., A stochastic-convective transport representation of dispersion in one-dimensional porous media systems, *Water Resour. Res., 18*(4), 1193–1214, 1982.

Sposito, G., W. A. Jury, and V. K. Gupta, Fundamental problems in the stochastic convection-dispersion model of solute transport in aquifers and field soils, *Water Resour. Res., 22*(1), 77–88, 1986.

Sudicky, E. A., An advection-diffusion theory of contaminant transport for stratified media, Ph.D. dissertation, 203 pp., Univ. of Waterloo, Waterloo, Ont., 1983.

Sudicky, E. A., A natural gradient experiment on solute transport in a sand aquifer: Spatial variability of hydraulic conductivity and its role in the dispersion process, *Water Resour. Res.*, this issue.

Sudicky, E. A., J. A. Cherry, and E. O. Frind, Migration of contaminants in groundwater at a landfill: A case study, 4, A natural-gradient dispersion test, *J. Hydrol., 63*, 81–108, 1983.

D. L. Freyberg, Department of Civil Engineering, Terman Engineering Center, Stanford University, Stanford, CA 94305.

(Received June 24, 1985;
revised April 9, 1986;
accepted April 21, 1986.)